Geological Magazine

www.cambridge.org/geo

Original Article

Cite this article: Chen G, Liu R, Deng T, and Wang L (2021) Bimodal magmatism produced by delamination: geochemical evidence from late Palaeozoic volcanic rocks from the Yili Block, Western Tianshan, Northwestern China. *Geological Magazine* **158**: 1059–1073. https://doi.org/10.1017/S0016756820001090

Received: 24 November 2019
Revised: 29 August 2020
Accepted: 9 September 2020
First published online: 27 October 2020

Keywords:
bimodal magmatism; A-type affinity of felsic volcanic rocks; extensional tectonic setting; delamination

Author for correspondence:
Rui Liu, Email: liurui35@mail.sysu.edu.cn

Bimodal magmatism produced by delamination: geochemical evidence from late Palaeozoic volcanic rocks from the Yili Block, Western Tianshan, Northwestern China

Genwen Chen[1], Rui Liu[2], Teng Deng[3] and Lixing Wang[4]

[1]CAS Key Laboratory of Mineralogy and Metallogeny, Guangzhou Institute of Geochemistry, Chinese Academy of Sciences, Guangzhou 510640, China; [2]School of Resources and Environmental Engineering, Shandong University of Technology, Zibo 255000, China; [3]State Key Laboratory of Nuclear Resources and Environment, East China University of Technology, Nanchang 330013, China and [4]Guangzhou Marine Geological Survey, Guangzhou 510760, China

Abstract

The Western Tianshan orogenic belt is essential for understanding the evolution of the Central Asian orogenic belt. However, no agreement exists among geologists about its tectonic environment during the Late Palaeozoic. The volcanic rocks of the Yishijilike and Wulang Formation in the Yili Block, Western Tianshan, formed in the Late Carboniferous to Early Permian, mainly consist of a bimodal suite of basalts – basaltic andesites and rhyolites, with only some intermediate rocks. Mafic rocks are slightly enriched in light rare earth elements (LREE) and depleted in Nb, Ta, Zr and Hf, suggesting a subduction-modified depleted mantle source. Some mafic samples in the Early Permian bimodal volcanic rocks have high Ti contents with relatively high concentrations of Nb and high field strength elements (HFSE) and low contents of heavy rare earth elements (HREE). These rocks are similar to the continental flood basalts, which suggests that they formed from an asthenospheric mantle. This paper indicates that mafic members were created by the partial melting of the asthenospheric mantle material and subduction-modified lithospheric mantle mixture. Some rhyolites and dacites in the Wulang formation were enriched in Ga, Nb, Zr, Ce and Y and depleted in Sr and Eu. Additionally, they showed fractionation of rare earth elements (REE) with negative Eu anomalies, which is indicative of an A-type affinity of felsic rocks. The genesis of mafic members and an A-type affinity of felsic members indicate that the Late Carboniferous – Early Permian magmatism in the Western Tianshan area formed as a result of an extensional setting. This study also reveals bimodal magmatism produced by delamination in an extensional tectonic setting.

1. Introduction

The Central Asian Orogenic Belt (CAOB) is a giant Palaeozoic orogenic belt located between the East European – Siberian Craton and the Tarim / North China cratons (Zhu *et al.*, 2005; Wang *et al.*, 2006). The western Tianshan, located on the southwestern side of the CAOB (Fig. 1a), is an essential Late Palaeozoic orogenic belt (Windley *et al.*, 1990; Gao *et al.*, 1998) and a typical accretion-type orogenic belt (Xiao *et al.*, 2009). As an essential part of the western Tianshan, the Yili – Central Tianshan Block 'recorded' the evolution of the CAOB during subduction, ocean closure and extension of the post-orogenic phase during the late Palaeozoic. The granites of the Yili – Central Tianshan Block, as well as the basalts, andesites and dacites of the late Devonian – early Carboniferous Dahalajunshan Formation, were interpreted as formed there in an island arc setting associated with the southern subduction of the North Tianshan ocean in the late Palaeozoic (Zhu *et al.*, 2005; Qian *et al.*, 2006; Wang *et al.*, 2006; Yang *et al.*, 2006; Xia *et al.*, 2011; An *et al.*, 2013). The late Carboniferous to Early Permian volcanic rocks in the Yili – Central Tianshan Block contain a suite of basalts – basaltic andesites and rhyolites, with only some intermediate rocks, formed in an extensional environment (GW Chen *et al.*, 2015; BX Chen *et al.*, 2019; Ning *et al.*, 2019).

Agreement on aspects of the dynamic background of these bimodal volcanic rocks is not yet achieved among scientists. Some scholars believe that the volcanics in the west of Awulale Mountain, which is located in the centre of the Yili – Central Tianshan Block (Fig. 1b), formed because of lithospheric delamination during the post-collision stage (Li *et al.*, 2012; Zhao *et al.*, 2013; Chen *et al.*, 2015), while others suggest that these bimodal volcanic rocks may be related to the Permian Tarim mantle plume (Xia *et al.*, 2004). One group of scholars believe that large-scale magmatic activity in the Awulale region was a result of the breakage of the subducted slab, triggered by the upwelling of the depleted asthenospheric mantle (Long *et al.*, 2011;

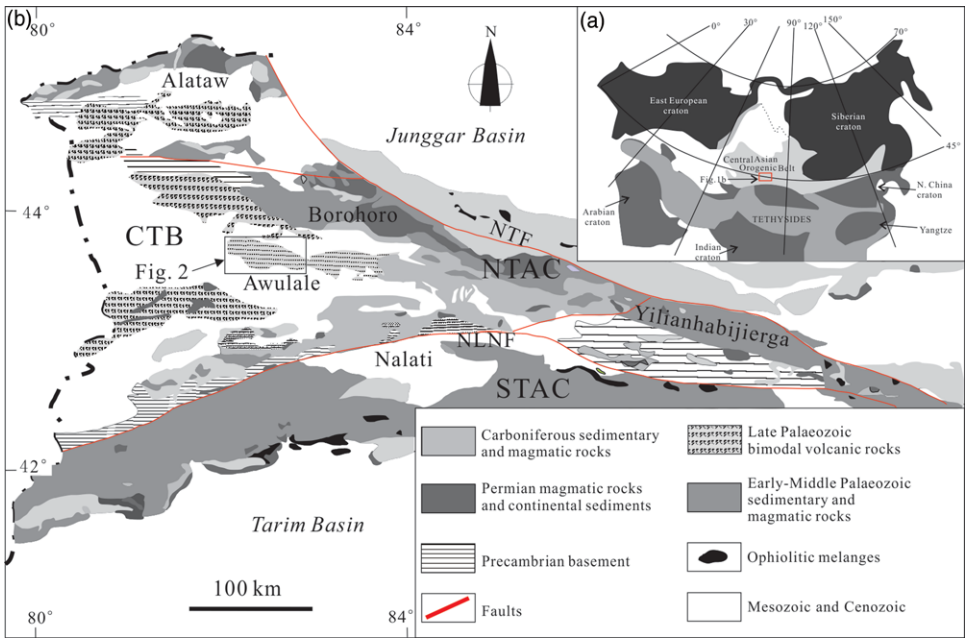

Fig. 1. (Colour online) (a) Location of the western Tianshan in the CAOB. (b) Map showing tectonics and volcanic rocks in the western Tianshan (adopted from Gao *et al.* 2009). CTB: Yili – Central Tianshan Block; NTAC: North Tianshan accretionary complex; NTF: North Tianshan fault; STAC: South Tianshan accretionary complex; STF: South Tianshan fault.

Ding *et al.*, 2014; Feng & Zhu, 2019) or an overlaying depleted mantle source, located over the possible mantle plume formed during the early Permian (Long *et al.*, 2012).

Awulale Mountain has the most complete Carboniferous–Permian strata in the western Tianshan. The suite of late Carboniferous – early Permian bimodal volcanics located in the Awulale region contains extensive high-Ti, high-Nb basalts and rhyolite with A-type chemical characteristics. Together with the regional geological features, this paper re-evaluates the genesis and geological background of these bimodal volcanic rocks.

2. Geological background

The Western Tianshan area is a critical component of the CAOB (Fig. 1a). It is tectonically subdivided into the North Tianshan accretionary complex (NTAC), the Yili – Central Tianshan Block (CTB) and the South Tianshan accretionary complex (STAC), bounded by the North Tianshan fault (NTF) and the South Tianshan fault (STF), respectively (Fig. 1b) (Li *et al.*, 2006; Gao *et al.*, 2009; Qian *et al.*, 2009; Xiao *et al.*, 2013; Jiang *et al.*, 2014; Yang *et al.*, 2018; Chen *et al.*, 2020).

The NTAC is composed of early Carboniferous ophiolitic complexes and the Carboniferous volcano-sedimentary rocks, which (e.g. Bayingou ophiolite) are the remains of the North Tianshan Ocean (Xu *et al.*, 2005; Wang *et al.*, 2006; Yang *et al.*, 2018). The age of the plagio-granites from the Bayingou ophiolite was determined as 324.8 ± 7.1 Ma (Xu *et al.*, 2006). The granodiorite age intruding the ophiolitic complexes was 316 ± 3 Ma (Han *et al.*, 2010), which indicates oceanic basin closure before 300 Ma.

The Yili – Central Tianshan Block, situated in the central part of the Western Tianshan orogenic belt, is a triangular area, bordered by the North Tianshan fault (NTF) and the Nalati Fault along with its NTAC and STAC parts, respectively. It contains Proterozoic amphibolite facies metamorphic rocks dated at 880–970 Ma using U–Pb zircon ages (Chen *et al.*, 1999; Hu *et al.*, 2000; Wang *et al.*, 2014) with Palaeozoic intrusive igneous and thick late Palaeozoic volcano-sedimentary rocks. The volcanic rocks are present in the northern Nalati Mountain, Yishijilike Mountain, Awulale Mountain and Dahalajunshan Mountain. Voluminous Carboniferous–Permian plutonic rocks are also well-developed in the Yili – Central Tianshan Block (Wang *et al.*, 2007; Li *et al.*, 2010; Zhu *et al.*, 2011). The intrusive rocks in the Yili – Central Tianshan Block mainly include three periods: early Palaeozoic, late Devonian – early Carboniferous and late Carboniferous – early Permian. The early Palaeozoic intrusive rocks contain mostly calc-alkaline granite resulted from northward subduction of the Southern Tianshan Ocean in the early Palaeozoic and the metaluminous and peraluminous granite, associated with the Yili – Central Tianshan Block and the Tarim plate collision, which are present in the southern margin of the Nalati Mountains 400–490 Ma in age (Yang *et al.*, 2006; Zhang *et al.*, 2008; Zhu *et al.*, 2011; Liu *et al.*, 2016, 2020; Liu & Chen, 2018, 2020). Devonian – early Carboniferous granites are calc-alkaline granites mainly found in the southern margin of the North Tianshan and Nalati Mountains. They formed by the southern subduction of the North Tianshan Ocean and the northern subduction of the southern Tianshan Ocean (Chen *et al.*, 2020). The late Palaeozoic intrusive rocks (formed 310–390 Ma), distributed in the northern Yili – Central Tianshan Block, are mostly granodiorites (Tang *et al.*, 2008; XH Zhang *et al.*, 2008; ZH Zhang *et al.*, 2010). During the Late Carboniferous – early Permian, a suite of quartz albite porphyry, monzogranite, potassium feldspar granite and diabase intruded in the Yili – Central Tianshan Block. These granitoids are characterized by adakites (Li *et al.*, 2019) and A-type granite (Tang *et al.*, 2008; Liu & Chen, 2018, 2020). Similar to the late Carboniferous – early Permian bimodal volcanic rocks, these rocks limit the time of the post-orogenic phase of the western Tianshan.

The area of interest is located west of Awulale Mountain (Fig. 1b). Awulale Mountain contains mainly late Palaeozoic volcanic and intrusive rocks (Fig. 1b). Its stratigraphy is composed of Carboniferous to Permian sequences (250–330 Ma in age) (Zhu *et al.*, 2005; Zhao *et al.*, 2009; Li *et al.*, 2013; Liu *et al.*, 2016; Liu & Chen, 2018). According to the regional lithology, Awulale Mountain can be divided into (1) the western section, which mostly consists of Permian volcanics 251–298 Ma in age with minor Carboniferous volcanic rocks and some Late Palaeozoic intrusions as shown in Figure 2a (Zhao *et al.*, 2006;

https://doi.org/10.1017/S0016756820001090 Published online by Cambridge University Press

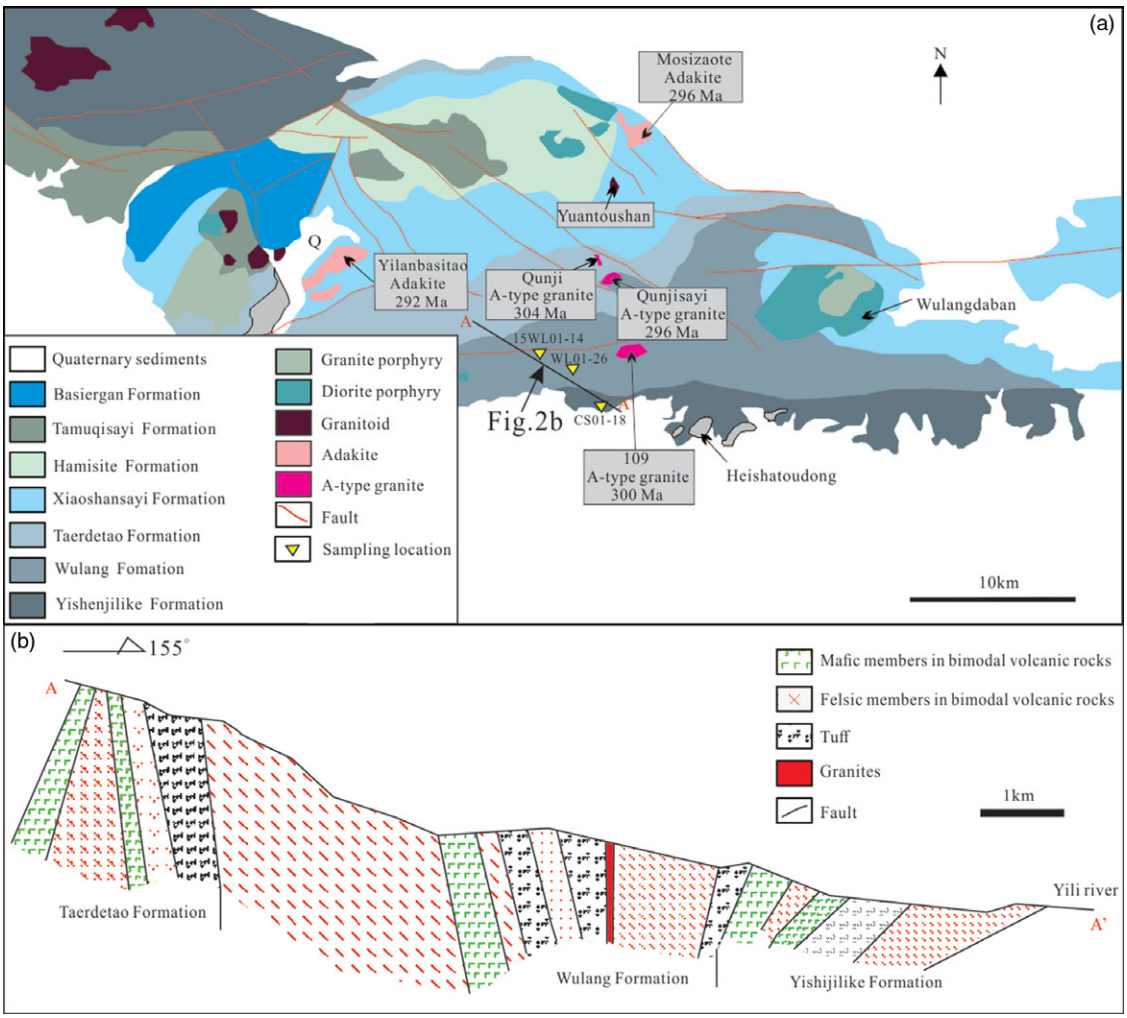

Fig. 2. (Colour online) (a) Geological map of western Awulale Mountain (adopted from Li *et al.* 2013). Data on ages are from Li *et al.* (2013, 2015) and Liu & Chen (2020) as well as from our unpublished data. (b) Cross-section of the Yishijilike, Wulang and Taerdetao Formations located in the western Awulale Mountain region.

Li *et al.*, 2013; Liu *et al.*, 2016; Liu & Chen, 2020), and (2) the eastern section, which contains Carboniferous volcanic rocks 312–327 Ma in age, some late Palaeozoic intrusions (284–312 Ma in age) and some Permian volcanic rocks (261–271 Ma in age) (Zhu *et al.*, 2005; Feng & Zhu, 2019). The Carboniferous rocks in the Awulale region include the Yishijilike Formation, and the Permian rocks in this region include Wulang, Taerdetao, Xiaoshansayi and Tamuqisayi Formations. Plutons (290–330 Ma) are widely distributed in Awulale Mountain (Zhu *et al.*, 2005). They include some adakitic plutons with zircon U–Pb 291–296 Ma in age (Li *et al.*, 2019; our unpublished data), A-type granites with zircon U–Pb 296–303 Ma in age (Liu *et al.*, 2016; Liu & Chen, 2020) and diabase dikes with K–Ar 310 Ma in age (Yao, 1993) (Fig. 2a).

Distinct deformation structures, developed in Awulale Mountain, include folds, faults and dome structures. During the Early Carboniferous, E–W-trending structure patterns formed. There are incongruous and angular folds in the Akeshake Formation below the Yishijilike Formation (Li *et al.*, 2010). Many NW- and NE-trending tensional faults formed in the study area during the late Carboniferous period. E–W-trending tectonics during the Permian was transformed by NW- and NE-trending tectonic belts. Thus, these tectonic movements formed many faults, domes and folds, which controlled the distribution of the intrusions.

3. Field relationships and petrography

Stratigraphy in the study area mainly includes the Yishijilike, Wulang, Taerdetao, Xiaoshansayi, Hamisite, Tamuqisayi and Basiergan Formations (Fig. 2a), corresponding to decreasing deposition/eruption ages. The Yishijilike Formation consists of rhyolite and small amounts of basalt, intruded by porphyritic granites. The age of rhyolites in the Yishijilike obtained using the laser ablation – inductively coupled plasma – mass spectrometry (LA-ICP-MS) zircon U–Pb dating technique is *c.* 303 Ma (Ning *et al.*, 2019). The Wulang Formation mainly contains volcanic rocks, including dacite, rhyolite, basalt and felsic tuff. It covers the Yishijilike Formation conformably (Fig. 2b). The eruption age of the Wulang Formation volcanic rocks was closer to 291 Ma, dated by the LA-ICP-MS zircon U–Pb ageing technique (Ding *et al.*, 2014). The Taerdetao Formation consists of bimodal volcanic rocks and covers the Wulang Formation conformably (Fig. 2b). The Xiaoshansayi, Hamisite and Tamuqisayi Formations are composed of sedimentary rocks. The Xiaoshansayi Formation mainly consists of sandstone, siltstone, and mudstone, and covers the Taerdetao Formation conformably. The Hamisite Formation, composed of conglomerate, sandstone and silty marl, is located in parallel to and conformably overlies the Xiaoshansayi Formation. The Tamuqisayi Formation mainly consists of

https://doi.org/10.1017/S0016756820001090 Published online by Cambridge University Press

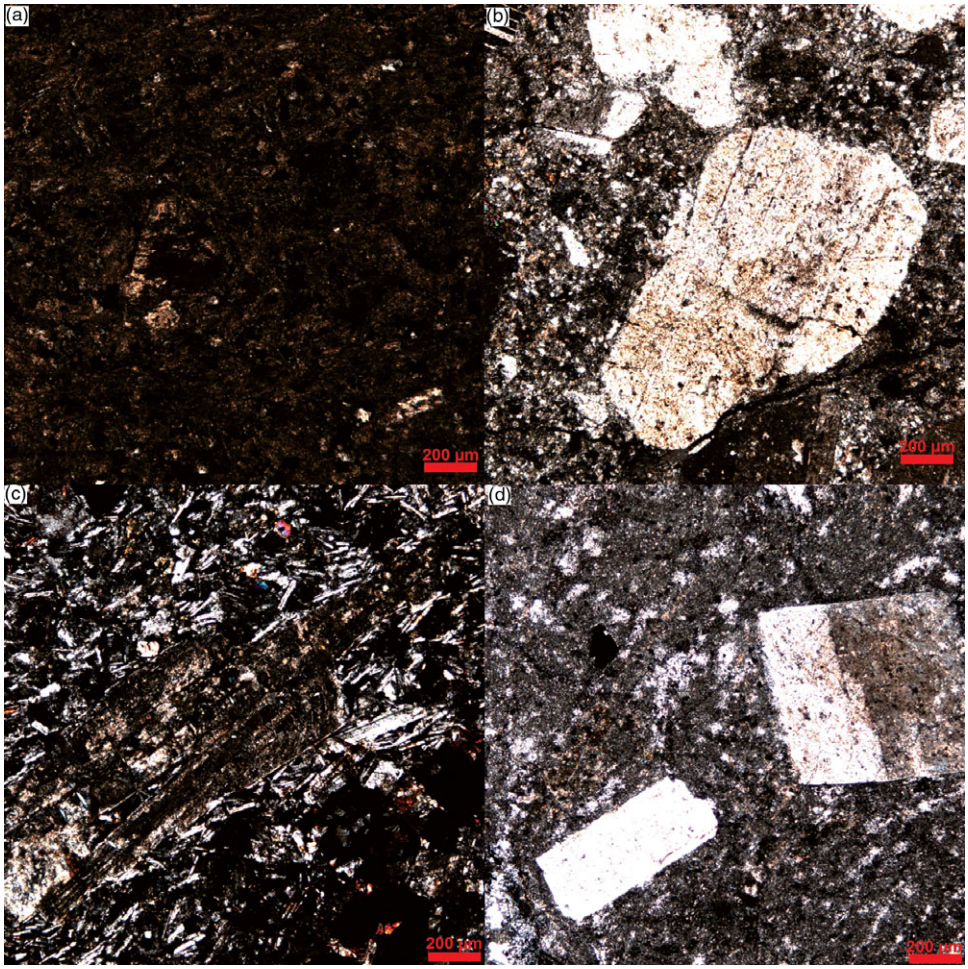

Fig. 3. (Colour online) Micrographs showing mineralogical characteristics of the bimodal volcanic rocks from the Yishijilike and Wulang Formations: (a, c) basaltic rocks, (b, d) rhyolitic rocks.

conglomerate, sandstone and mudstone and covers the Hamisite Formation conformably. The Basiergan Formation, composed of boulder conglomerate, charcoal mudstone and silty mudstone, covers the Tamuqisayi Formation conformably. Tectonics in this area is mainly characterized by folds and faults. Due to the structural compression, stratigraphy in this area can be described as having steep dips.

Fresh volcanic rock samples for petrological and geochemical analyses were collected from the geological sections of the Yishijilike and Wulang Formations and from several scattered outcrops along the ridge (Fig. 2a). Volcanic rocks collected in two successive formations can reveal the continual evolution of the regional geology. Twenty-one samples (5 mafic rocks and 16 felsic rocks) and 30 samples (17 mafic rocks and 13 felsic rocks) were collected from the Yishijilike Formation and Wulang Formation, respectively. These samples were collected every 10–20 m to confirm that they represent the formation's full volcanic stratigraphy. As dacite and felsic tuff represent only a small part of the stratigraphy, the felsic rocks of these formations are mainly composed of rhyolites. The basalts in the Yishijilike Formation are dark grey and possess a porphyritic texture with phenocrysts of plagioclase. The groundmasses include fine-grained plagioclase, pyroxene, amphibole and Fe–Ti oxides (Fig. 3a). The felsic volcanic rocks in the Yishijilike Formation include dacites and rhyolites, which are either aphyric or porphyritic with 5–10 % phenocrysts. As the difference between dacites and rhyolites is not obvious in outcrops and under a microscope, we classify them as felsic rocks. The main phenocryst phase of the felsic rocks is plagioclase (Fig. 3b). Mafic mineral phenocrysts, which are observed rarely, include clinopyroxene, hornblende and biotite (Fig. 3b). The basalts from the Wulang Formation are also dark grey and contain clinopyroxene, plagioclase and Fe–Ti oxides (Fig. 3c). Shapes of the plagioclase grains are subhedral and lath-like (Fig. 3c). Rhyolitic rocks from the Wulang Formation are purple and possess porphyritic texture with phenocrysts of K-feldspar (Fig. 3d). Major phases of the groundmasses are K-feldspar, quartz and plagioclase, while minor ones are titanite, zircon and apatite. These rocks were affected by the hydrothermal weathering, demonstrated by the replacement of clinopyroxene by other minerals and sericitization of feldspar (Fig. 3).

4. Analytical techniques

After the petrographic examination, some freshly collected rock pieces were crashed ultrasonically first in 5 wt % HNO_3 solution and then in distilled water, after which the samples were dried and examined. Any visually detected contamination was removed by hand. Another batch of freshly collected rocks was prepared for elemental and isotopic analyses. Rocks were split into small chips, ultrasonicated in distilled water, dried and then ground to powder. Sample pieces with pores or slight alterations (especially basalt and basaltic andesite samples) were soaked in 4N HCl for 1 h to remove carbonates, rinsed with distilled water, dried and then ground to powder.

https://doi.org/10.1017/S0016756820001090 Published online by Cambridge University Press

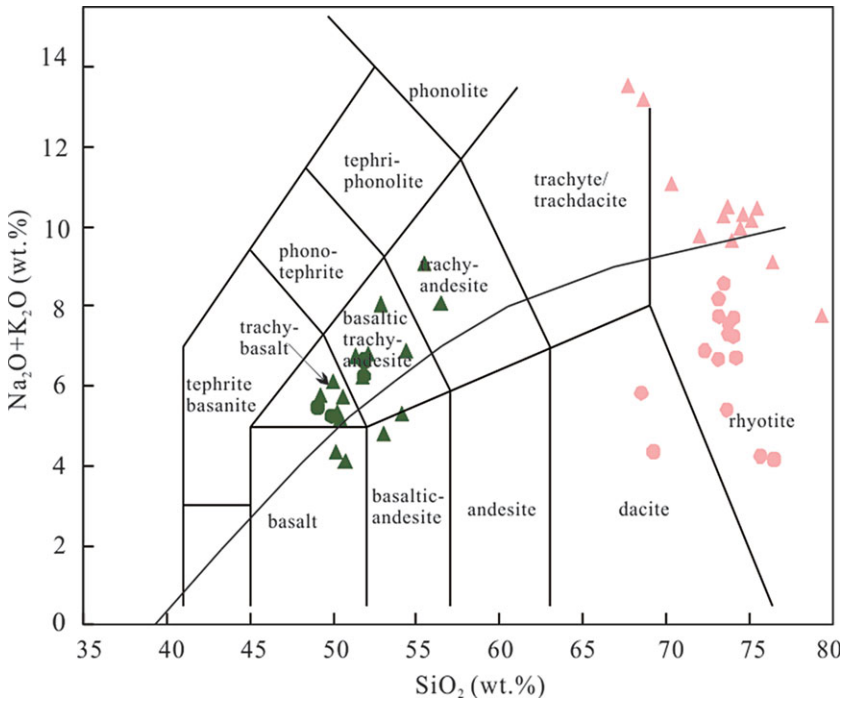

Fig. 4. (Colour online) The total content of alkali metal oxides plotted as a function of the SiO_2 content. Magma series classification is taken from Irvine and Baragar (1971). Green circles: mafic rocks from the Yishijilike Formation; pink circles: felsic rocks from the Yishijilike Formation; green triangles: low-Ti mafic rocks from the Wulang Formation; green rhombus: high-Ti mafic rocks from the Wulang Formation; pink triangle: felsic rocks from the Wulang Formation. Data for the felsic rocks from the Wulang Formation are taken from Ding *et al.* (2014).

4.a. Whole-rock major and trace elements measurements

Whole-rock major element compositions were analysed using X-ray fluorescence (XRF) at the Guangzhou Institute of Geochemistry, Chinese Academy of Sciences (GIG CAS), China. The analytical accuracy of the major element determination was ±1–2 %. We used the gravimetric method to analyse the losses on ignition (LOI). Whole-rock trace element contents were obtained by ICP-MS at the GIG CAS. Fifty milligrams of the powdered samples was dissolved in HF/HNO_3 mixture for 7 days at 100 °C in a screw-top Teflon beaker. An internal Rh standard was used to monitor drift in mass response during counting. USGS BCR-1 standard was used for elemental concentration calibration. The accuracy of the analysis was ±5 %.

4.b. Whole-rock Sr–Nd isotope

Sr and Nd isotopes were determined by ISOPROBE-T thermal ionization mass spectrometer at the Beijing Research Institute of Uranium Geology. For this purpose, powders were completely dissolved in Savilex bombs using standard procedures. Sr and Nd were isolated using a two-column method. Some Sr fractions were additionally purified by a third column. $^{143}Nd/^{144}Nd$ ratios were normalized against $^{146}Nd/^{144}Nd$ standard value equal to 0.7219. $^{87}Sr/^{86}Sr$ ratios were normalized to the $^{86}Sr/^{88}Sr$ standard value equal to 0.1194, and checked against the NBS-987 standard (equal to 0.710250 ± 0.000007). Our measurements on the SHINESTU Nd standard yielded a value equal to 0.512118 ± 0.000003.

5. Results

5.a. Whole-rock chemical compositions

The whole-rock chemical compositions are listed in Supplementary Table S1 (in the supplementary material available online at https://doi.org/10.1017/S0016756820001090). Some samples showed relatively high LOI (>3 wt %), indicating that these volcanic rocks underwent weathering and alteration after the eruption.

After accounting to LOI and recalculating, the results to 100 % of SiO_2 content were plotted as a function of total K_2O and Na_2O contents. The resulting diagram demonstrates good bimodal geochemical distribution (Fig. 4). Five mafic rocks from the Yishijilike Formation are classified as basaltic trachyandesite (three samples) and trachybasalt (two samples) types. Sixteen samples of the Yishijilike Formation felsic rocks fell into a dacite–rhyolite field, fourteen of which were classified as rhyolites, and two as dacites. Seventeen samples in the Wulang Formation show a compositionally expanded basalt – trachybasalt – basaltic trachyandesite – basaltic andesite – trachyandesite suite. Felsic samples in the Wulang Formation are potassic trachytes (two samples with 11 wt % K_2O) and rhyolites (13 samples).

Mafic rocks in the Yishijilike Formation are characterized by low silica contents (46.2–51.4 wt %), moderate MgO (4.48–5.66 wt %), CaO (3.99–7.11 wt %) and TiO_2 (1.04–1.16 wt %) levels and relatively high Al_2O_3 (16.1–17.9 wt %), $K_2O + Na_2O$ (4.71–6.39 wt %) and P_2O_5 (0.27–0.29 wt %) levels. The mafic rocks in the Yishijilike Formation are slightly enriched in light rare earth elements (LREE) judging by the $(La/Yb)_N$ value in the 4.2–5.0 range. These rocks also demonstrate small Eu negative anomalies because the Eu/Eu* ratios are in the 0.85–1.00 range (Fig. 5a). Samples show pronounced Pb positive anomalies (Fig. 5a). REE patterns for these mafic rocks are flat. The primitive mantle-normalized diagram shows that these mafic rocks are enriched with large-ion lithophile elements (LILE) (such as Th and U) and depleted in Nb, Hf, Zr and Ta (Fig. 5b).

The chondrite-normalized diagram of the felsic rocks in the Yishijilike Formation demonstrates enrichment of these rocks in LREE (judging by the La_N/Yb_N ratio equal to 1.1–7.6) and severe depletion by Eu (based on the corresponding Eu/Eu* ratio equal to 0.22–0.52; Fig. 5c). Samples showed pronounced Pb positive anomalies (Fig. 5c). At the same time, the primitive mantle-normalized diagram shows that these samples were

https://doi.org/10.1017/S0016756820001090 Published online by Cambridge University Press

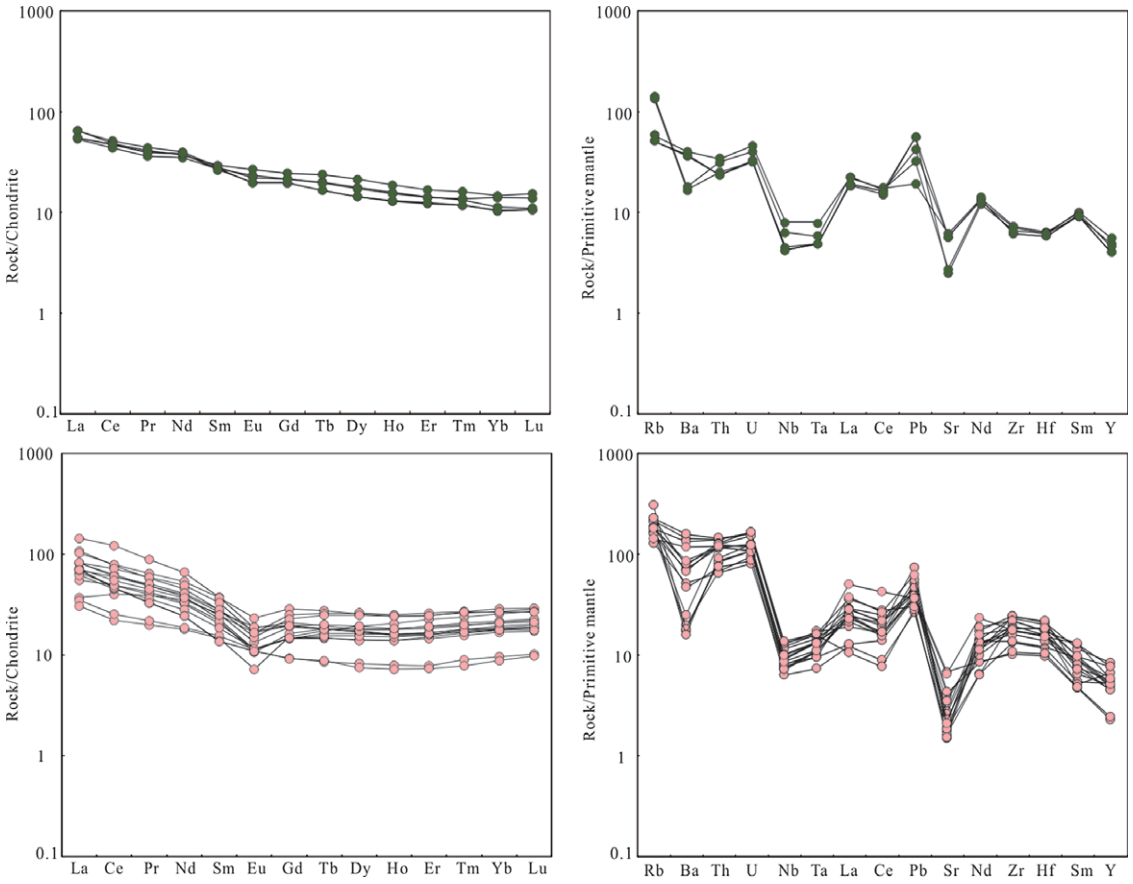

Fig. 5. (Colour online) Chondrite-normalized REE and primitive mantle-normalized trace element patterns of bimodal volcanic rocks from the Yishijilike Formation. Green circles: mafic rocks; pink circles: felsic rocks. Average chondrite and primitive mantle-normalizing values were taken from Sun and McDonough (1989).

enriched with LILEs (such as Rb, U and Th) and depleted in Ba, Sr, Nb and Ta (Fig. 5d).

There are two basalt groups present in the Wulang Formation: high-Ti basalt (TiO_2 = 2.26–2.34 wt %) and low-Ti basalt (0.62–1.21 wt %). The high-Ti basalts have total Fe_2O_3 content (12.80–13.34 wt %) higher than in the low-Ti basalts (5.65–11.1 wt %). All mafic rocks possess higher Na (than K) contents and are also slightly enriched with LREEs ($(La/Yb)_N = 3.22–5.26$) with almost no negative Eu anomalies ($Eu/Eu^* = 0.83–1.07$) and with relatively flat REE patterns (Fig. 6a). Some basalts have relatively high Nb ($>7 \times 10^{-6}$), as well as P and high field strength elements (HFSE) contents, which is typical for the Nb-enriched basalts (Sajona *et al.*, 1993). Samples show distinct positive Pb anomalies (Fig. 6a). The primitive mantle-normalized diagram demonstrates that mafic rocks are enriched with Rb, Th and U and depleted in Nb, Ta, Zr and Hf (Fig. 6b).

Felsic rocks in the Wulang Formation are also enriched with LREE associations (with $La_N/Yb_N = 3.04–6.87$). A chondrite-normalized diagram of the felsic rocks from the Wulang Formation shows negative Eu values (with $Eu/Eu^* = 0.46–0.50$; Fig. 6c). Samples show pronounced positive Pb anomalies (Fig. 6c). The primitive mantle-normalized diagram (Fig. 6d) demonstrates LILE-enriched and Ba-, Sr-, Nb- and Ta-depleted felsic rocks, which is similar to the results observed for the Yishijilike Formation.

5.b. Nd isotopic compositions

The distribution of Nd isotope is given in Table 1. Previous studies showed that when the initial $(^{87}Sr/^{86}Sr)i$ ratio was affected by the hydrothermal alteration (Menzies *et al.*, 1993) or the $^{87}Rb/^{86}Sr$ ratio was high, it became not credible (Jahn *et al.*, 2000, 2009). However, Nd isotopes are relatively stable and unaffected by these processes; therefore, the $\epsilon_{Nd}(t)$ values are still credible (Menzies *et al.*, 1993; Mahoney *et al.*, 1998). Thus, in this work, we focus on the Nd isotopic composition in the bimodal volcanics.

Initial $^{143}Nd/^{144}Nd$ ratios in the mafic samples from the Yishijilike Formation are in the 0.512646–0.512685 range. Initial ratios are calculated using the age equal to 303 Ma (Ning *et al.*, 2019). Corresponding $\epsilon_{Nd}(t)$ values are in the 1.54–2.42 range (Fig. 7). $^{143}Nd/^{144}Nd$ ratio and $\epsilon_{Nd}(t)$ values for the felsic rocks from the Yishijilike Formation are in the 0.512594–0.512709 and 1.62–2.70 ranges, respectively (Fig. 7).

$^{143}Nd/^{144}Nd$ ratios in the mafic samples from the Wulang Formation are in the 0.512744–0.512985 range. Initial ratios were calculated using 291 Ma age (Ding *et al.*, 2014). Corresponding $\epsilon_{Nd}(t)$ values are in the 4.35–7.41 range (Fig. 7). $^{143}Nd/^{144}Nd$ ratio and $\epsilon_{Nd}(t)$ values for the felsic rocks from the Wulang Formation are in the 0.512652–0.512765 and 4.66–5.33 ranges, respectively (Fig. 7).

6. Discussion

6.a. Hydrothermal alteration effects

Hydrothermal alteration effects of the volcanic rocks with LOI > 3 wt % should be taken into account. Because of higher enhanced mobility during surface modification, incompatible element contents might change during post-eruption processes. Zr and Hf are typically immobile during the low-grade alteration

https://doi.org/10.1017/S0016756820001090 Published online by Cambridge University Press

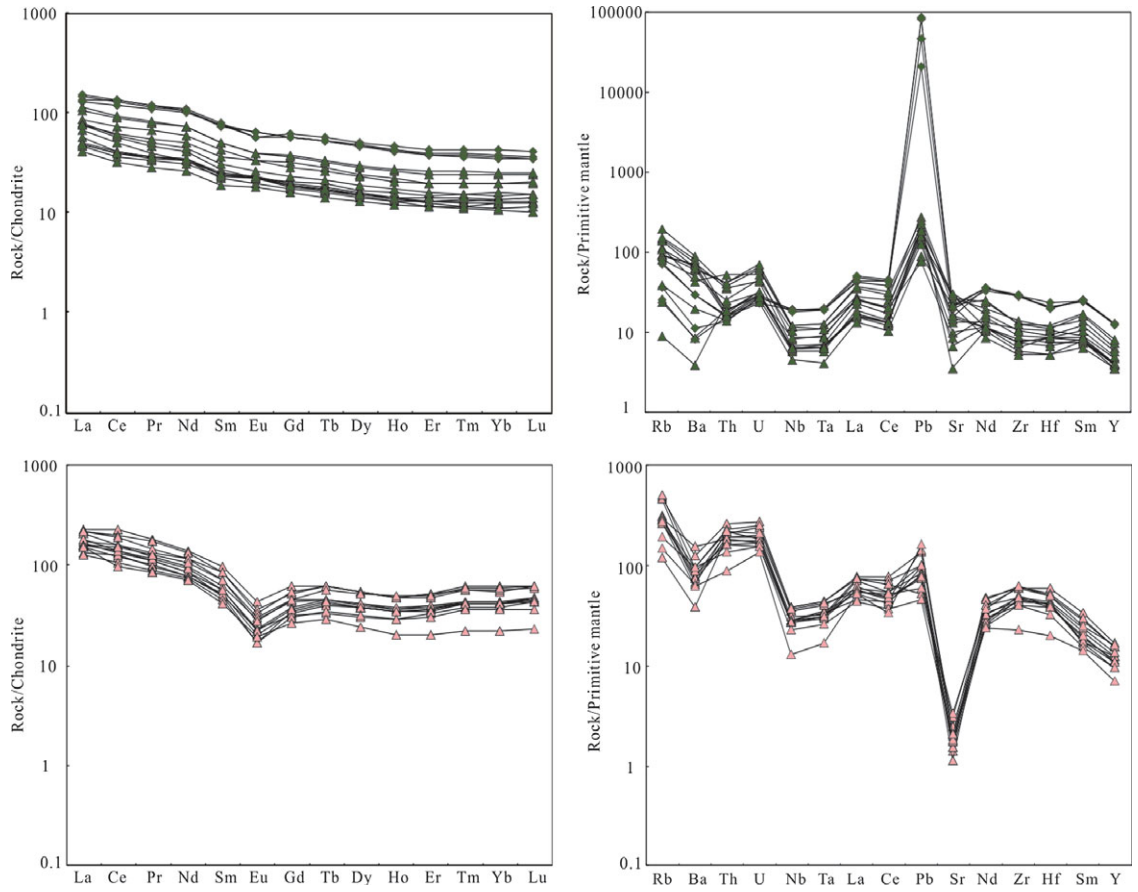

Fig. 6. (Colour online) Chondrite-normalized REE and primitive mantle-normalized trace element patterns of bimodal volcanic rocks from the Wulang Formation. Green triangles: low-Ti mafic rocks; green rhombus: high-Ti mafic rocks; pink triangles: felsic rocks. Average chondrite and primitive mantle-normalizing values are taken from Sun and McDonough (1989).

and metamorphism (Gibson *et al.*, 1982; Pearce *et al.*, 1992). Therefore, they were used to reveal the movements of other elements during post-eruption processes. Zr and Th correlated very well with La, Nb, Nd and U contents (Supplementary Figs S1 and S2a (in the supplementary material available online at https://doi.org/10.1017/S0016756820001090)). Thus, La, Nb, Nd and U were also relatively immobile during post-magmatic processes. In addition, considerable scatter was observed when Rb content was plotted as a function of the Th content (Fig. S2b). Additionally, no correlation between Sr and Th was observed for the mafic samples (Fig. S2c), which indicates the mobility of Rb and Sr during post-stage alternation. A considerable scatter was also observed when Ba content was plotted as a function of the Th content (Fig. S2d), which suggests Ba mobility during alternation.

Overall variations of HFSEs, such as Th, Zr, Nb, Hf and Y, and REE, could be attributed to the magmatism, which can be used to reveal the rock geochemical characteristics. However, Rb, Sr and Ba contents were very likely affected by the alteration processes. Thus, they cannot be used to study the petrogenesis of the rocks evaluated in this work.

6.b. Petrogenesis

6.b.1. Mafic rocks

The mafic volcanic rocks from the Yishijilike and Wulang Formations possess relatively low concentrations of MgO, Ni, Cr and Co. Thus, these rocks are characterized by low $Mg^{\#}$ values, which are significantly lower than the values for the primary basaltic melts, indicating that they probably experienced some crystal fractionation (e.g. Wilson, 1989b; Green, 2015; Green & Falloon, 2015; Mitchell & Grove, 2015). In addition, as illustrated in Supplementary Figure S3 (in the supplementary material available online at https://doi.org/10.1017/S0016756820001090), SiO_2 content positively correlates with Na_2O, Th, Nb and Zr contents (Supplementary Fig. S3a–d), but negatively with MgO, Cr and Ni contents (Supplementary Fig. S3e, f), which is consistent with fractional crystallization effect.

The positive $\epsilon_{Nd}(t)$ values of the mafic end member in the Yishijilike Formation and Wulang Formation bimodal volcanics are in the +1.54 to +2.42 and +4.35 to +7.41 ranges, respectively (Fig. 7), indicating a depleted mantle source. The mafic volcanic rocks from the Yishijilike Formation and the low-Ti basalts in the Wulang Formation are LILE-enriched and HFSE-depleted (e.g. Nb and Ta), indicating a possibility for some subduction-related mantle metasomatism (Kuyumjian & Danni, 1991). Most rocks have Nb/La (0.4–0.5) and Nb/Th (1.5–5.3) ratios below values of the typical normal mid-ocean ridge basalts (N-MORB) (with Nb/La and Nb/Th ratios equal to 1.0 and 19.5, respectively; Sun & McDonough, 1989) but similar to the values in the subduction-related magma (Nb/La = 0.53, Nb/Th = 3.10; Kelemen *et al.*, 2014). Furthermore, most mafic rocks possess high Th/Yb (1.29–3.22) but low Nb/Yb ratios (3.50–7.03) and deviate from the MORB – ocean island basalt (OIB) arrays (Fig. 8) of the subduction-modified lithospheric mantle plot (Pearce, 2008).

https://doi.org/10.1017/S0016756820001090 Published online by Cambridge University Press

Table 1. Nd isotope data for the bimodal volcanic rocks from the Yishijilike and Wulang Formations

Samples	Rocks	Sm (ppm)	Nd (ppm)	$^{147}Sm/^{144}Nd$	$^{143}Nd/^{144}Nd$	$SE_{(Nd)}$	$(^{143}Nd/^{144}Nd)_i$	ϵ_{Nd} (*t*)
CS01	rhyolite	5.07	23.03	0.134151	0.512594	0.000002	0.512322	1.62
CS02	rhyolite	4.32	19.77	0.13305	0.512616	0.000002	0.512346	2.09
CS04	basalt	4.35	18.58	0.142391	0.512652	0.000002	0.512363	2.42
CS06	basalt	4.50	17.26	0.158714	0.51264	0.000003	0.512318	1.54
CS07	rhyolite	2.39	8.74	0.166745	0.512696	0.000003	0.512358	2.32
CS10	rhyolite	2.26	8.43	0.163526	0.512709	0.000004	0.512377	2.70
CS11	rhyolite	5.68	25.12	0.137655	0.512652	0.000003	0.512373	2.61
WL14	rhyolite	3.82	19.22	0.120161	0.512765	0.000006	0.512536	5.33
WL15	rhyolite	3.82	14.52	0.158892	0.512837	0.000006	0.512534	5.28
WL27*	rhyolite	9.37	45.6	0.1242	0.512755	0.000009	0.51252	4.98
WL28*	rhyolite	14.5	65.2	0.1345	0.512758	0.000008	0.51250	4.66
WL29*	rhyolite	10.5	54.7	0.1161	0.512747	0.000010	0.51253	5.13
WL30	basalt	5.66	25.35	0.134962	0.512757	0.000006	0.512500	4.62
WL31	basalt	5.84	26.57	0.132816	0.512775	0.000007	0.512522	5.06
WL32	basalt	4.19	18.13	0.139656	0.512760	0.000006	0.512494	4.50
WL33	basalt	4.71	19.53	0.145929	0.512791	0.000005	0.512513	4.88
WL34	basalt	4.27	18.08	0.142718	0.512758	0.000006	0.512486	4.35
WL35	basalt	4.55	17.49	0.157282	0.512824	0.000005	0.512524	5.09
WL36*	basalt	2.65	8.62	0.1968	0.512985	0.000012	0.52160	6.77
WL37*	basalt	4.12	16.40	0.1647	0.512834	0.000015	0.51251	5.05
WL38*	basalt	3.20	10.60	0.1958	0.512932	0.000010	0.51255	5.77
WL39*	basalt	2.75	9.04	0.1986	0.512262	0.000013	0.51187	7.41
WL40*	basalt	2.81	9.19	0.2021	0.513000	0.000010	0.51260	6.86
WL41*	basalt	5.19	22.30	0.1407	0.212779	0.000011	0.51250	4.90
WL42*	basalt	5.57	24.10	0.1397	0.512770	0.000006	0.51250	4.76
WL43*	basalt	4.88	21.10	0.1398	0.512760	0.000006	0.51249	4.56
WL44*	basalt	6.20	28.30	0.1325	0.512744	0.000009	0.51248	4.53
15WL01	basalt	11.26	48.94	0.1401	0.512701	0.000010	0.51242	3.47
15WL02	basalt	10.99	47.95	0.1340	0.512687	0.000011	0.51240	3.22

Note: $\epsilon_{Nd}(t) = [(^{143}Nd/^{144}Nd)_i/(^{143}Nd/^{144}Nd)_{CHUR} - 1] \times 10^4$, $(^{143}Nd/^{144}Nd)_{CHUR} = 0.512638$, $(^{147}Sm/^{144}Sm)_{CHUR} = 0.1967$.
$T_{DM} = 1/\sigma \times \ln(1 + [(^{143}Nd/^{144}Nd)_i - 0.51315]/[(^{147}Sm/^{144}Nd)_i - 0.2137]$, $t = 310$ Ma, $\lambda_{Sm} = 6.54 \times 10^{-12}$.
*Data from Ding (2014).

In addition, the Nb/Ta and Zr/Hf values for these mafic rocks were in the 15.0–18.8 and 30.9–43.9 ranges, respectively, which are similar to the analogous values for the primitive mantle equal to 17 ± 2 and 36.2 (Sun & McDonough, 1989). However, the mafic rocks possess variable $\epsilon_{Nd}(t)$ values (in the 1.54–7.41 range), suggesting that the source of mafic rocks is a heterogeneous mantle. Figure 7 shows $\epsilon_{Nd}(t)$ of basalts in the Wulang Formation plotted for the area between the Bayingou ophiolite, the Dahalajunshan Formation and the Yishijilike Formation. It demonstrates the tendency of crustal mixing, which may indicate that the depleted mantle source of basalts in the Early Permian Wulang Formation was mixed with the early underplated basalts. Four high-Ti basalts with high TiO_2 and Fe_2O_3 but low Al_2O_3 contents possessed chemical composition similar to the experimental fertile peridotite melt. Thus, the source of these rocks might be similar to the fertile mantle (Falloon *et al.*, 1988). Basalts with high TiO_2 contents are enriched with P, Zr, Nb, Ta and REE, with positive whole-rock $\epsilon_{Nd}(t)$ values (equal to +3.1 to +4.3), which is similar to continental flood basalts (Hornig, 1993; Farmer, 2013). Thus, they originated from an asthenospheric mantle source. Compared to other basaltic rocks, the high-Ti basalts show that they were not affected by the subduction-related fluids and/or melts (Fig. 8). The influence of the evolution of the mantle on Th and Ta is similar. In contrast, Th and Ta will be differentiated in the mantle wedge under the influence of the subduction zone fluid. As a result, Th will be strongly enriched in the magma (Wilson, 1989a). The Th/Ta ratio of high-Ti basalt samples in this area is equal to 0.50–1.73, similar to the Th/Ta ratio of MORB (0.75–2; Pearce, 1991). It is significantly lower than the values observed for the island arc basalt (which are in the 35 range) and in the upper crust

https://doi.org/10.1017/S0016756820001090 Published online by Cambridge University Press

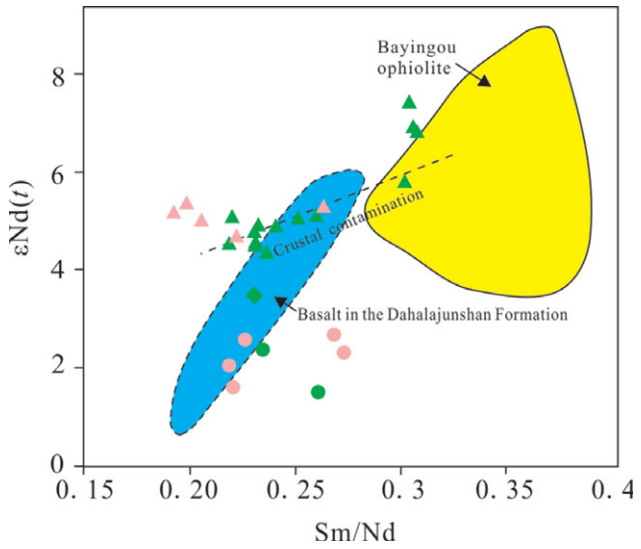

Fig. 7. (Colour online) Sm/Nd vs $\epsilon_{Nd}(t)$ diagrams. Green circles and pink circles represent mafic rocks and felsic rocks from the Yishijilike Formation, respectively; green triangles, green rhombus and pink triangles represent low-Ti mafic rocks, high-Ti mafic rocks and felsic rocks of the Wulang Formation, respectively. Data sources: Bayingou ophiolites (Xu *et al.* 2006; Chen *et al.* 2020); Dahalajunshan Formation basalt (Qian *et al.* 2006).

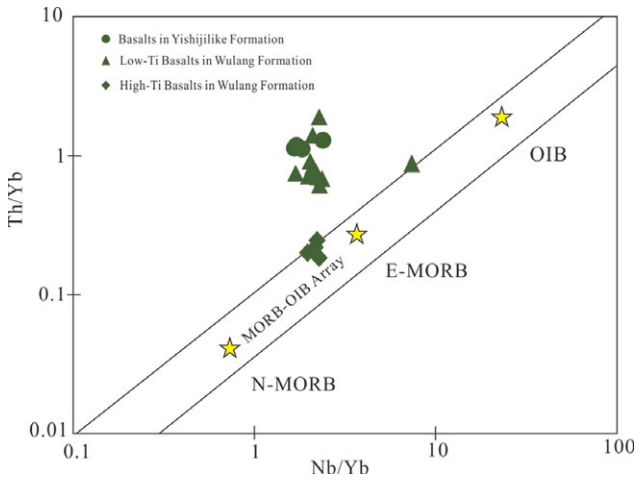

Fig. 8. (Colour online) Nb/Yb plotted on the Th/Yb diagram, adopted from Leat *et al.* (2002) and Pearce (2008). Data are for the mafic volcanics from the Yishijilike Formation (green circles) and the Wulang Formation (green triangles for low-Ti mafic rocks and green rhombus for high-Ti mafic rocks).

(with the value equal to 10). Thus, the source area of high-Ti basalt cannot be described as 'metasomatism by subduction fluid'. Therefore, the source of high-Ti basalt is different from other basalts. Compared with the typical asthenospheric mantle, Nb and Ta content in high-Ti basalt are slightly lower, which is typical for mantle depleted in trace elements. This may be related to the magma mixing with the lithospheric mantle. The Ti, Nb and Zr contents in basalts are generally high, indicating that the source is mixed with high-Ti, -Nb and -Zr material. SiO_2–TiO_2, SiO_2–Nb, TiO_2–Nb and TiO_2–Zr diagrams show that low-Ti end member is mixed with high-Ti end member (Fig. 9), indicating that the high-Ti basalt was indeed mixed with the lithospheric mantle. Therefore, the asthenosphere material was involved in the late Palaeozoic magmatism in this area.

The mafic rocks of the Yishijilike Formation and Wulang Formation possess flat HREE patterns (Figs 5a and 6a), which indicate no residual garnet presence during the partial melting of the mantle source. La/Yb ratios often reflect partial melting as well as the presence of spinels or garnets as predominant residual phases (Yang *et al.*, 2007). The basalt source is relatively shallow at low La/Yb ratios, especially when spinel is a dominant residual phase. Basalt may form because of the relatively large partial melting. In contrast, the high La/Yb ratios may reflect that the basalt source is relatively deep and that the garnet is the dominant residual phase in the source. Meantime, basalt may be formed by smaller melt fractions. In this study, the mafic rocks have low La/Yb (<7.49), $(La/Sm)_N$ (<2.23) and $(Tb/Yb)_N$ (<1.78) ratios while demonstrating relatively flat middle rare earth elements (MREE) and HREE patterns (Figs 5a and 6a). Thus, the source of basalt is relatively shallow: <60–70 km (Zhang *et al.*, 2008). Therefore, basalt very likely formed by partial melting of a mantle in the spinel field, which agrees with the moderate TiO_2 and total $Fe_2O_3{}^T$ concentrations in basalts. The composition of these mafic rocks is also consistent with the composition of the glasses obtained by partial melting of the natural anhydrous fertile spinel peridotite (e.g. Hirose & Kushiro, 1993).

6.b.2. Felsic rocks

SiO_2 in felsic volcanic rocks negatively correlated with TiO_2, MgO, $Fe_2O_3{}^T$, Al_2O_3 and CaO (Supplementary Fig. S4a–e (in the supplementary material available online at https://doi.org/10.1017/S0016756820001090)) contents, indicating that they experienced fractional crystallization (e.g. amphibole ± plagioclase ± Fe–Ti oxides). In addition, the P_2O_5 negatively correlated with SiO_2, suggesting apatite crystallization (Supplementary Fig. S4f (in the supplementary material available online at https://doi.org/10.1017/S0016756820001090)). The negative Eu anomalies in felsic rocks (Figs 5c and 6c) may be caused by (1) intensive fractional crystallization of feldspar during post-eruption processes, (2) strong negative Eu anomalies of magma sources or (3) large amounts of feldspar left in the melting residue (Zhang *et al.*, 2008). However, many geochemical variables (such as major and trace elements) show no linear correlation with SiO_2 in the felsic rocks, indicating no strong role of magma mixing or fractional assimilation crystallization in the felsic rock petrogenesis, which is consistent with the vague crystal differentiation of felsic rocks shown in Figure 10.

In general, the felsic suite rocks in bimodal volcanic rocks may be produced by fractional crystallization of associated basaltic magma (Sheth & Melluso, 2008) or by partial melting of crustal materials (Mahoney *et al.*, 2008). The mafic and felsic volcanics in the study area are temporally and spatially associated with each other. Geochemically, the trace element features of the felsic group and of the mafic rocks are similar. In addition, the felsic rocks from the Yishijilike Formation and Wulang Formation demonstrate moderate whole-rock Nd isotopic contents ($\varepsilon_{Nd}(t) = +1.62$ to $+2.09$ and $+2.61$ to $+5.33$, respectively), which correspond to their basalts (with $\varepsilon_{Nd}(t)$ equal to $+1.54$ to $+2.42$ and $+4.35$ to $+7.41$, respectively), suggesting that they could be genetically related by the fractional crystallization process, or indicating that the felsic rocks were produced by partial melting of juvenile basaltic crust (i.e. underplated basaltic crust), derived from the same mantle source. The fractionation of the basaltic melt should result in continuous compositions ranging from the unfractionated basalt to intermediate compositions to the rhyolite (Best & Christiansen, 2001). Field observations and sampling of the western Tianshan

https://doi.org/10.1017/S0016756820001090 Published online by Cambridge University Press

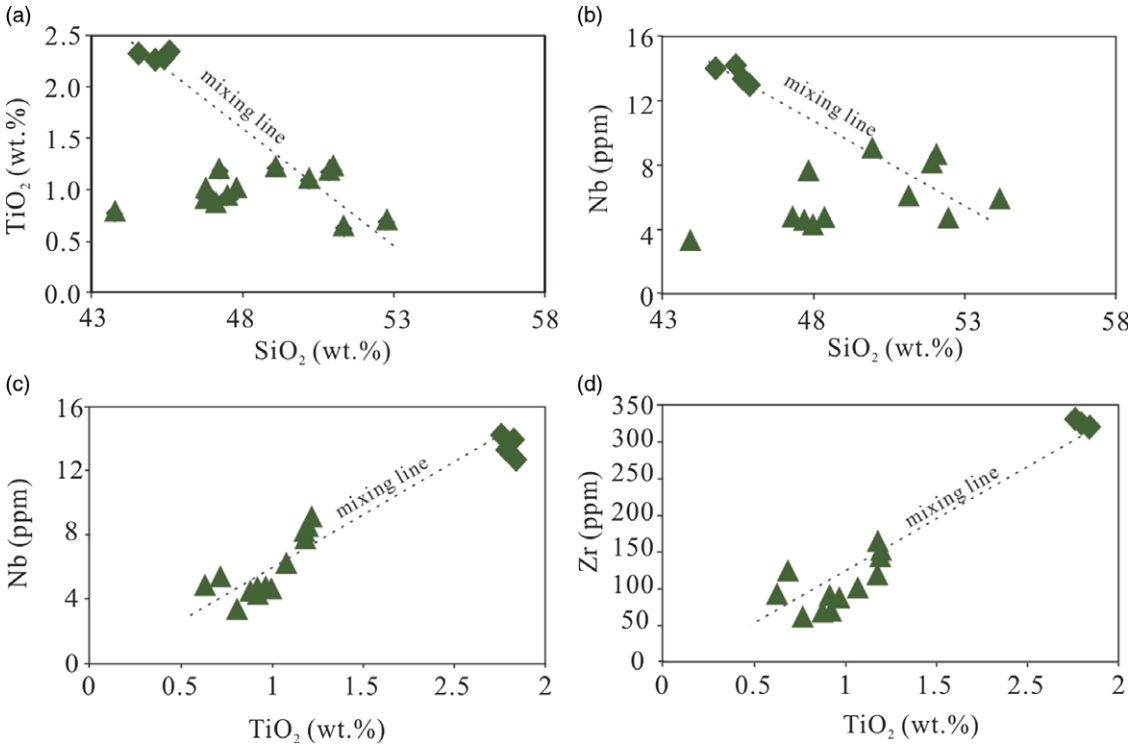

Fig. 9. (Colour online) SiO_2 contents plotted as a function of TiO_2 (a) and Nb (b) for mafic volcanic rocks from the Wulang Formation. TiO_2 contents plotted as a function of Nb (c) and Zr (d).

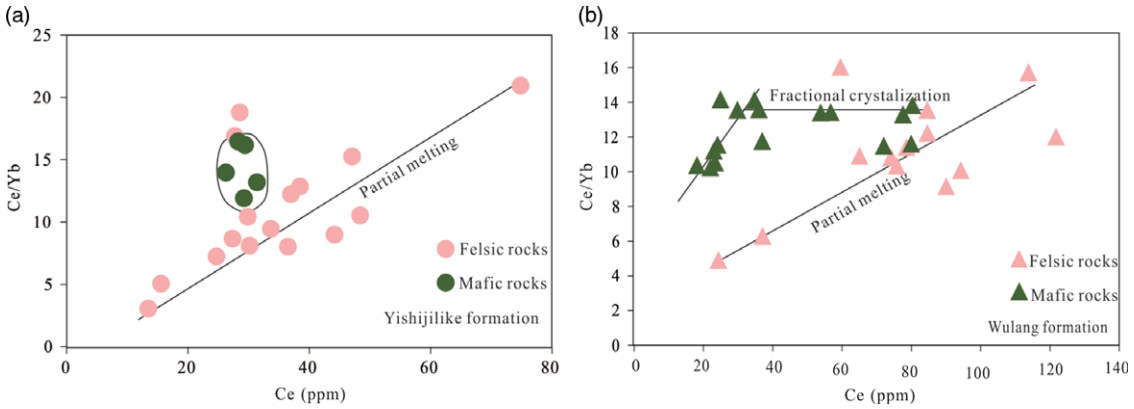

Fig. 10. (Colour online) Ce contents plotted as a function of Ce/Yb for volcanic rocks from the Yishijilike Formation (a) and from the Wulang Formation (b), adopted from Allegre and Minster (1978).

showed a large compositional gap between the basalt and the rhyolite. Many geochemical variables of the major and trace elements variations figures (shown in Supplementary Figs S1–4 (in the supplementary material available online at https://doi.org/10.1017/S0016756820001090)) show no linear correlation with SiO_2 in the felsic rocks, indicating no significant role of magma mixing or fractional assimilation crystallization in the felsic rock petrogenesis. This was corroborated by the Ce/Yb ratio plotted as a function of the Ce diagram (Fig. 10), in which the felsic rocks of the Yishijilike Formation and Wulang Formation follow the partial melting trend (and not the fractional crystallization trend) (Allegre & Minster, 1978). In addition, a diagram showing Nb distribution as a function of Ta and as a function of U demonstrates that basaltic rocks and felsic rocks are distributed along different evolutionary lines (Fig. 11), indicating that felsic volcanic rocks cannot be produced by fractional crystallization of basaltic magma, which implies that they formed by partial melting of the newly underplated basaltic crust.

The felsic rocks of the Wulang Formation possess extremely high FeO*/(FeO* + MgO), SiO_2, K_2O + Na_2O, Zr, Ga, REE and HFSE contents, which is indicative of their similarity to A-type felsic rocks (Collins *et al.*, 1982; Whalen et al. 1987). Whalen *et al.*, (1987) and Frost *et al.*, (2001) demonstrated that A-type granite could be distinguished from the I- and S-types by discrimination diagrams (shown in Fig. 12). In addition, using the Watson & Harrison (1983) formula, we calculated the Zr saturation temperature (T_{Zr}) in the felsic rocks of the Wulang Formation. The values of T_{Zr} (899–1009 °C) agree with experimental

https://doi.org/10.1017/S0016756820001090 Published online by Cambridge University Press

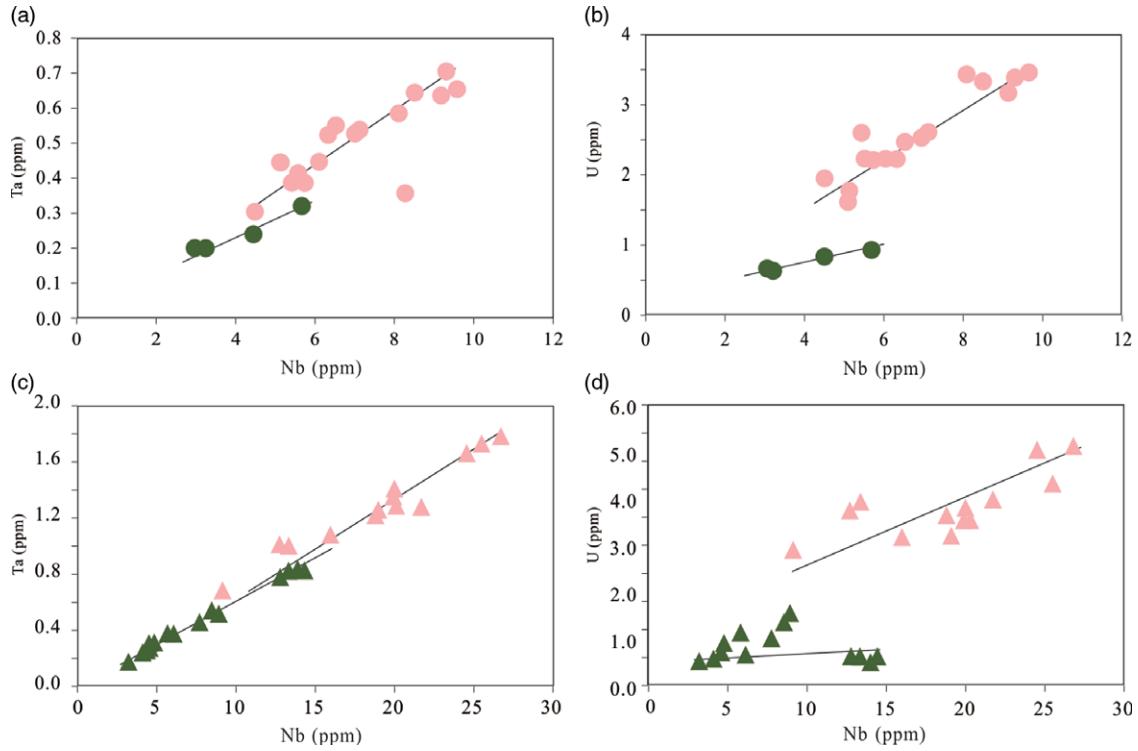

Fig. 11. (Colour online) Nb contents plotted as a function of Th and U for volcanic rocks from the Yishijilike Formation (a, b) and from the Wulang Formation (c, d).

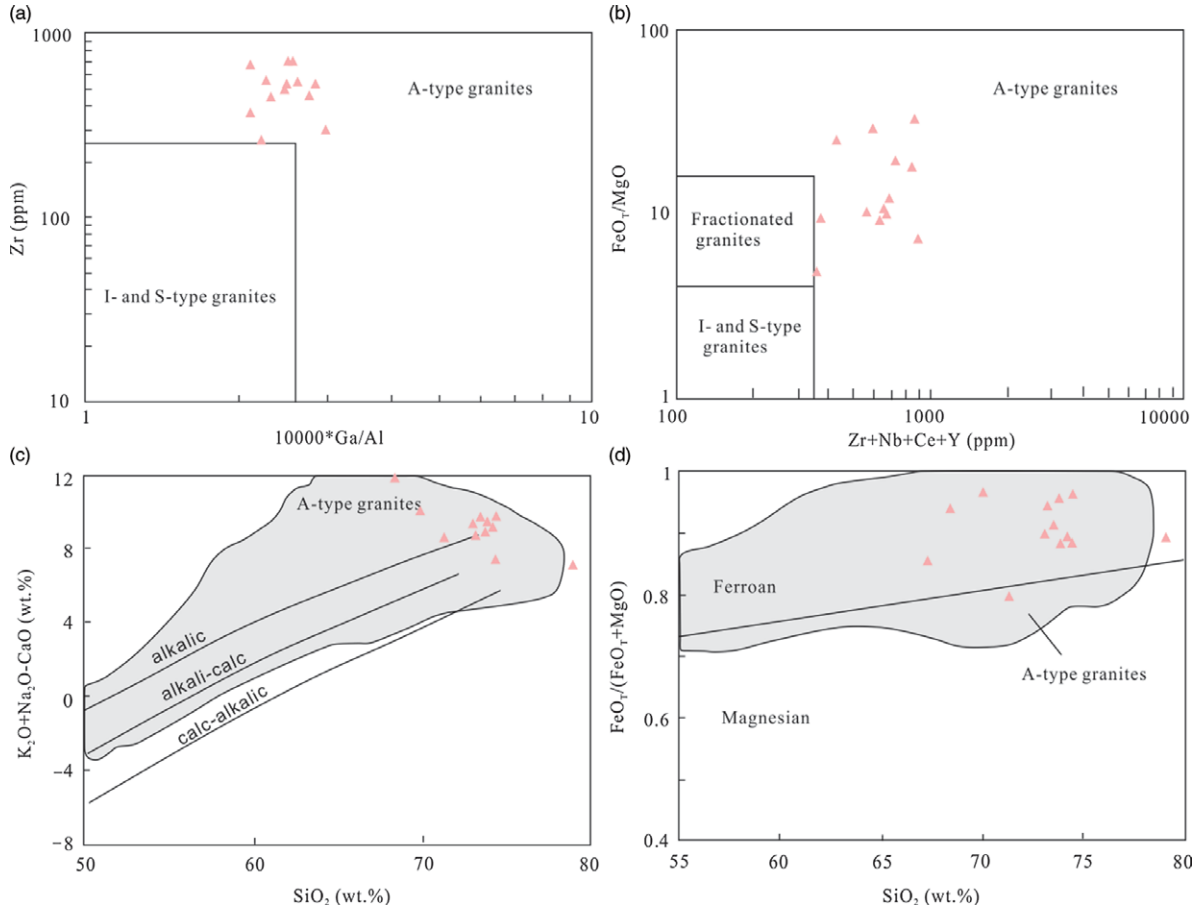

Fig. 12. (Colour online) 10 000*Ga/Al plotted as a function of Zr (a), and Zr + Nb + Ce + Y plotted as a function of FeO_T/MgO (b), adopted from Whalen *et al.* (1987). SiO_2 plotted as a function of $K_2O + Na_2O$ – CaO (c) and $FeO_T/(FeO_T + MgO)$ (d), adopted from Frost *et al.* (2001).

https://doi.org/10.1017/S0016756820001090 Published online by Cambridge University Press

constraints (>830 °C) of the corresponding A-type granites temperature (Clemens *et al.*, 1986). Thus, these felsic rocks have A-type granite affinities.

A-type granites and their volcanic counterparts can be created as a result of (1) fractionation of mantle-derived alkaline mafic magmas (Eby, 1990; Litvinovsky *et al.*, 2002; Bonin, 2007), (2) melting of a quartz–feldspathic crustal source and/or mixing of the mafic and felsic crustal sources (Kerr & Fryer, 1993), (3) partial melting of dry low crustal residual granulates, which triggered the formation of I-type magmas (Collins *et al.*, 1982; Whalen *et al.*, 1987; King *et al.*, 1997) or (4) partial melting of a mantle-based newly formed parental basaltic magma (e.g. Frost & Frost, 1997).

As mentioned above, the felsic rocks of the Wulang Formation did not undergo significant fractional crystallization. In addition, A-type granites in the study area have low compatible elements, such as MgO (0.09–0.72 wt %), Cr (1.36–17.6 ppm), Co (0.52–6.85 ppm) and Ni (0.96–7.31 ppm), indicating that these magmas did not originate from the mantle. Low Al content and A/CNK value suggest that these granites are unlikely to be formed by the partial melting of the metamorphic sedimentary rocks. Meanwhile, these felsic rocks with characteristics of A-type granite have higher K_2O contents. Additionally, almost all samples have higher K_2O contents than Na_2O contents, which is similar to the magma formed by the crustal matter (Martin *et al.*, 2005). By taking into account the characteristics of Nd isotopic composition, it is evident that the felsic volcanics in the studied formations most likely formed by the partial melting of the juvenile basic lower crust. In addition, Liu *et al.*, (2016) proposed that the $f_{Sm/Nd}$ and t_{DM} (~0.69 Ga) of A-type granites in the Qunji are similar to those in granites distributed in the north of the CAOB. Thus, A-type granites in Qunji also originated from the juvenile basaltic lower crust.

6.c. Tectonic implications

Late Carboniferous – early Permian bimodal volcanic rocks, A-type granites and their volcanic counterparts are common in the western Tianshan. Previous studies suggested that these bimodal volcanic rocks might be: (1) related to the Permian Tarim mantle plume (Xia *et al.*, 2004) or (2) resulted from the breakage of the subducted slab triggered by the upwelling of the depleted asthenospheric mantle (Long *et al.*, 2011; Ding *et al.*, 2014; Feng & Zhu, 2019). It is also possible that the depleted mantle source overlaid the possible mantle plume (Long *et al.*, 2012). In general, mafic rocks in bimodal magmatic suites formed during the post-collisional and/or in-plate extensional settings and frequently consisted of tholeiitic gabbros and basalts. At the same time, felsic members in bimodal magmatic suites, formed in these conditions, usually possess geochemical characteristics of A-type granites (Hildreth *et al.*, 1991; Turner *et al.*, 1992; Frost & Frost, 1997; Frost *et al.*, 1999; Bonin *et al.*, 2004).

As mentioned above, the formation of basalts in the Wulang Formation involved asthenospheric material, and early underplated basalts were added into their source. Additionally, the felsic rocks in the Wulang Formation possess the geochemical characteristics of A-type granite, created by the partial melting of juvenile basaltic lower crust under high temperatures. We speculate that there are two possible causes for this high geothermal gradient: the uplift of asthenosphere material, and the detachment of the thickened lithosphere into the asthenosphere. The dynamic mechanisms, causing the rise of asthenospheric materials, mainly include oceanic ridge subduction, subducted plate fracture (Feng & Zhu, 2019) or the retraction roll-back of the subducted plate (Gvirtzman & Nur, 1999), and lithospheric detachment disturbance (Altunkaynak, 2007; Zhang *et al.*, 2017). Numerous data indicate that starting from the late Carboniferous, this area had entered the stage of post-orogenic extensional development (Han *et al.*, 2005; Mao *et al.*, 2008; Tang *et al.*, 2008; YJ Li *et al.*, 2009; Tong *et al.*, 2010; Yang *et al.*, 2010; Chen *et al.*, 2015; NB Li *et al.*, 2015; Liu *et al.*, 2016; Liu & Chen, 2020). In addition, magmatism caused by ocean-ridge subduction, slab rollback and slab breakage would be distributed along a narrow linear zone. At the same time, lithospheric delamination would affect a much wider area (Altunkaynak, 2007). Geological facts indicate that volcanics in the late Palaeozoic are common in the western Tianshan. Therefore, the mechanism associated with plate subduction can be ruled out. It is then more likely that the detachment of the thickened lithosphere caused the uplift of the asthenospheric material. New research results on the western Tianshan also support the existence of detachment of lithosphere and asthenospheric uplift in the late Palaeozoic (Xia *et al.*, 2004; Feng *et al.*, 2019; Li *et al.*, 2019). The early Carboniferous Akeshake Formation showed a broad and evident regional angular unconformity with the late Carboniferous Yishejilike Formation. Complex incongruous folds, angular fold, strong wrinkling, and regional ductile faults occurred within the Akeshake Formation, which was produced in the southern tropical and subtropical palaeogeographic region. The Akeshake Formation was created in the island arc and back-arc basin under a compressive tectonic system. Simultaneously, the late Carboniferous bimodal volcanic alkalic rocks and sedimentary formation were produced in a typical northern palaeogeographic region, which contained a suite of continental rift volcanic–sedimentary formation formed in the regional tectonic environment. Tectonic deformation is extremely weak (Li *et al.*, 2010). In addition, Permian terrestrial red molasse and coal-measure strata developed in the Yili basin, indicating rapid entering of the post-collision extension stage by the Tianshan area during the early Permian. Therefore, we believe that the bimodal magmatism was produced by delamination in an extensional tectonic setting.

7. Conclusions

Geological characteristics collected in the field and geochemical data obtained in the laboratory indicate that volcanics in the Yishijilike Formation and Wulang Formation from the Western Awulale area, Western Tianshan, are bimodal. Geochemical and isotopic compositions suggest that the mafic members in bimodal volcanic rocks resulted from partial melting of subduction-modified lithospheric mantle mixed with the asthenospheric mantle. The felsic rocks formed by partial melting of the newly underplated mafic lower crust. These typical bimodal volcanics very likely formed in a post-collisional extensional environment, indicating that the Awulale area already existed during its intraplate evolution stage in the Late Carboniferous period. These observations indicate that the bimodal magmatism was induced by the underplate of the asthenospheric mantle in reaction to the lithospheric mantle detachment and the extensional environment.

Supplementary material. To view supplementary material for this article, please visit https://doi.org/10.1017/S0016756820001090

Acknowledgements. Financial support for this work was provided by the Second Tibetan Plateau Scientific Expedition and Research Program (STEP) (Grant No. 2019QZKK0803), Deep Resources Exploration and Mining, a Special Project in the Framework of National Key R&D Program of China

(2017YFC0602302), the Fundamental Research Funds for the Central Universities (Project Nos. 191gpy75), the Open-Cooperation Fund of Key Laboratory of Mineralogy and Metallogeny, Guangzhou Institute of Geochemistry, Chinese Academy of Sciences (KLMM20190204) and the Guangdong Basic and Applied Basic Research Foundation (2020A1 515010906). We are also grateful to the editor Kathryn Goodenough for her assistance as well as to anonymous reviewers, whose comments and suggestions improved our paper.

Conflict of interest. None.

References

Allegre CG and Minster JF (1978) Quantitative models of trace element behavior in magmatic processes. *Earth and Planetary Science Letters* **38**, 1–25.

Altunkaynak S (2007) Collision-driven slab breakoff magmatism in northwestern Anatolia, Turkey. *Journal of Geology* **115**, 63–82.

An F, Zhu YF, Wei SN and Lai SC (2013) An Early Devonian to Early Carboniferous volcanic arc in North Tianshan, NW China: geochronological and geochemical evidence from volcanic rocks. *Journal of Asian Earth Sciences* **8**, 100–13.

Best MG and Christiansen EH (2001) *Igneous Petrology*. Oxford: Blackwell Science.

Bonin B (2007) A-type granites and related rocks: evolution of a concept, problems and prospects. *Lithos* **97**, 1–29.

Bonin B, Ethien R, Gerbe MC, Cottin JY, Féraud G, Gagnevin D, Giret A, Michon G and Moine B (2004) The Neogene to Recent Rallier-du-Baty nested ring complex, Kerguelen Archipelago (TAAF, Indian Ocean): stratigraphy revisited, implications for cauldron subsidence. In *Physical Geology of High-Level Magmatic Systems* (eds C Breitkreuz and N Petford), pp. 125–49. Geological Society of London, Special Publication no. 234.

Chen BX, Xu SL, Zhou NW, Bai QJ, Huang JH and Zheng Y (2019) Zircon U–Pb chronology and Hf isotopic compositions of the Early Permian bimodal volcanic rocks from Wulang Formation in Jiamante area of Western Tianshan, Xinjiang. *Geological Journal of China Universities* **25**, 364–76 (in Chinese with English abstract).

Chen CM, Lu HF, Jia D, Cai DS and Wu SM (1999) Closing history of the southern Tianshan oceanic basin, western China: an oblique collisional orogeny. *Tectonophysics* **302**, 23–40.

Chen GW, Deng T, Liu R, Xia H and Liu Q (2015) Geochemistry of bimodal volcanic rocks in Permian Taerdetao Formation in Awulale area of western Tianshan, Xinjiang. *Acta Petrologica Sinica* **31**, 105–18 (in Chinese with English abstract).

Chen GW, Yang JX, Liu R, Wang K, Wang LX and Wang K (2020) Geochemistry of mafic volcanics in the Bayingou ophiolitic mélange, Western Tianshan, NW China: implications for magma genesis and tectonic setting. *Lithos* **352–353**, 105292.

Clemens JD, Holloway JR and White AJR (1986) Origin of an A-type granite: experimental constraints. *American Mineralogist* **71**, 317–24.

Collins WJ, Beams SD, White AJR and Chappell BW (1982) Nature and origin of A-type granites with particular reference to southeastern Australia. *Contributions to Mineralogy and Petrology* **80**, 189–200.

Ding ZX, Xue CJ, Zhao XB, Yan YH, Yaxiaer Y, Feng B, Luo H, Zu B, Zhang Q and Dai ZJ (2014) Geochronology, geochemistry and petrogenesis of the Early Permian rhyolite and its constraints on the lithosphere deep processes. *Earth Science Frontiers* **21**, 196–210.

Eby GN (1990) The A-type granitoids: a review of their occurrence and chemical characteristics and speculations on their petrogensis. *Lithos* **26**, 115–34.

Falloon, TJ, Green, DH, Hatton, CJ and Harris, KL (1988) Anhydrous partial melting of a fertile and depleted peridotite from 2 to 30 kb and application to basalt petrogenesis. *Journal of Petrology* **29**, 1257–82.

Farmer L (2013) Continental basaltic rocks. In *Treatise on Geochemistry, vol. 4*, 2nd ed. (eds H Holland and K Turekian), pp. 75–110. Elsevier.

Feng B, Xue CJ, Zhao XB, Wang B and Zhang E (2019) Geochemistry and zircon U–Pb age of the Permian radial diabase dyke from southern Xinyuan area, Western Tianshan Mountains, Xinjiang, and their geological significance. *Geological Bulletin of China* **38**, 1028–39.

Feng WY and Zhu YF (2019) Petrogenesis and tectonic implications of the late Carboniferous calc-alkaline and shoshonitic magmatic rocks in the Awulale mountain, western Tianshan. *Gondwana Research* **76**, 44–61.

Frost BR, Barnes CG, Collins WJ, Arculus RJ, Ellis DJ and Frost CD (2001) A geochemical classification for granitic rocks. *Journal of Petrology* **42**, 2033–48.

Frost CD and Frost BR (1997) Reduced rapakivi-type granites: the tholeiite connection. *Geology* **25**, 647–50.

Frost CD, Frost BR, Chamberlain KR and Edwards BR (1999) Petrogenesis of the 1.43 Ga Sherman batholith, SE Wyoming, USA: a reduced, rapakivi-type anorogenic granite. *Journal of Petrology* **40**, 1771–802.

Gao J, Li MS, Xiao XC, Tang YQ and He GQ (1998) Paleozoic tectonic evolution of the Tianshan Orogen, northwestern China. *Tectonophysics* **287**, 213–31.

Gao J, Long LL, Klemd R, Qian Q, Liu DY, Xiong XM, Su W, Liu W, Wang YT and Yang FQ (2009) Tectonic evolution of the South Tianshan Orogen and adjacent regions, NW China: geochemical and age constraints of granitoid rocks. *International Journal of Earth Sciences* **98**, 1221–38.

Gibson IL, Kirkpatrick RJ, Emmerman R, Schmincke HU, Pritchard G, Oakley PJ, Thorpe RS and Marriner GF (1982) The trace element composition of the lavas and dikes from a 3-km vertical section through the lava pile of eastern Iceland. *Journal of Geophysical Research: Solid Earth* **87**, 6532–46.

Green DH (2015) Experimental petrology of peridotites, including effects of water and carbon on melting in the Earth's upper mantle. *Physics and Chemistry of Minerals* **42**, 95–122.

Green DH and Falloon TJ (2015) Mantle-derived magmas: intraplate, hot-spots and mid-ocean ridges. *Science Bulletin* **60**, 1873–900.

Gvirtzman Z and Nur A (1999) The formation of Mount Etna as the consequence of slab rollback. *Nature* **401**, 782–5.

Han BF, Guo ZJ, Zhang ZC, Zhang L, Chen JF and Song B (2010) Age, geochemistry, and tectonic implications of a late Paleozoic stitching pluton in the North Tian Shan suture zone, western China. *Geological Society of America Bulletin* **122**, 627–40.

Han BF, Ji JQ, Song W, Chen LH and Zhang L (2005) Late Paleozoic vertical growth of continental crust around the Junggar Basin, Xinjiang, China (Part I): timing of post-collisional plutonism. *Acta Petrologica Sinica* **22**, 1077–86 (in Chinese with English abstract).

Hildreth WES, Halliday AN and Christiansen RL (1991) Isotopic and chemical evidence concerning the genesis and contamination of basaltic and rhyolitic magma beneath the Yellowstone Plateau volcanic field. *Journal of Petrology* **32**, 63–138.

Hirose K and Kushiro I (1993) Partial melting of dry peridotites at high pressures: determination of compositions of melts segregated from peridotite using aggregates of diamond. *Earth and Planetary Science Letters* **114**, 477–89.

Hornig I (1993) High-Ti and Low-Ti tholeites in the Jurassic Ferrar Group, Antarctica. *Geologisches Jahrbuch. Reihe E, Geophysik* **47**, 335–69.

Hu AQ, Jahn BM, Zhang GX and Zhang QF (2000) Crustal evolution and Phanerozoic crustal growth in northern Xinjiang: Nd-Sr isotopic evidence Part I: isotopic characterisation of basement rocks. *Tectonophysics* **328**, 15–51.

Irvine TN and Baragar WRA (1971) A Guide to Chemical Classification of the Common Volcanic Rock. *Canadian Journal of Earth Sciences* **8**, 523–548.

Jahn BM, Litvinovsky BA, Zanvilevich AN and Reichow M (2009) Peralkaline granitoid magmatism in the Mongolian–Transbaikalian Belt: evolution, petrogenesis and tectonic significance. *Lithos* **113**, 521–39.

Jahn BM, Wu F and Chen B (2000) Granitoids of the Central Asian Orogenic Belt and continental growth in the Phanerozoic. *Earth and Environmental Science Transactions of the Royal Society of Edinburgh* **91**, 181–93.

Jiang T, Gao J, Klemd R, Qian Q, Zhang X, Xiong XM, Wang XS, Tan Z and Chen BX (2014) Paleozoic ophiolitic mélanges from the South Tianshan Orogen, NW China: geological, geochemical and geochronological implications for the geodynamic setting. *Tectonophysics* **612–613**, 106–27.

Kelemen PB, Hanghj K and Greene AR (2014) One view of the geochemistry of subduction-related magmatic arcs, with an emphasis on primitive andesite and lower crust. *Treatise on Geochemistry* (Second Edition) **4**, 749–806.

https://doi.org/10.1017/S0016756820001090 Published online by Cambridge University Press

Kerr A and Fryer BJ (1993) Nd isotope evidence for crust-mantle interaction in the generation of A-type granitoid suites in Labrador, Canada. *Chemical Geology* **104**, 39–60.

King PL, White AJR, Chappell BW and Allen CM (1997) Characterization and origin of aluminous A-type granites from the Lachlan Fold Belt, southeastern Australia. *Journal of Petrology* **38**, 371–91.

Kuyumjian RM and Danni JC (1991) Geoquímica de anfibolitos da seqüência de Juscelândia, Goiás: implicações geotectônicas. *Revista Brasileira de Geociências* **21**, 218–23.

Leat PT, Riley TR, Wareham CD, Millar IL, Kelley SP and Storey BC (2002) Tectonic setting of primitive magmas involcanic arcs: an example from the Antarctic Peninsula. *Journal of the geological society* **159**, 31–44.

Li JY, He GQ, Xu X, Li HQ, Sun GH, Yang TN, Gao LM and Zhu ZX (2006) Crustal tectonic framework of northern Tianshan and adjacent regions and its formation. *Acta Petrologica Sinica* **80**, 149–168 (in Chinese with English abstract).

Li NB, Niu HC, Qiang S, Jiang YH, Zeng LJ, Yang WB and Pei ZJ (2013) Zircon U–Pb geochronology and geochemistry of post-collisional granitic porphyry from Yuantoushan, Nileke, Xinjiang. *Acta Petrologica Sinica* **29**, 3402–12 (in Chinese with English abstract).

Li NB, Niu HC, Shan Q and Yang WB (2015) Two episodes of Late Paleozoic A-type magmatism in the Qunjisayi area, western Tianshan: petrogenesis and tectonic implications. *Journal of Asian Earth Sciences* **113**, 238–53.

Li NB, Niu HC, Yang WB, Lai CK and Zhao ZH (2019) Orogenic root delamination induced by eclogitization of thickened lower crust in the Chinese Western Tianshan: constraints from adakites. *JGR – Solid Earth* **124**, 11089–104.

Li XY, Xu XY, Sun JM, Li ZP, Bai JK and Zhang XB (2012) Shallow granitic intrusions in the Nileke area of the Western Tianshan Mountains: geochemical characteristics and formation era. *Geological Bulletin of China* **31**, 1939–48.

Li YJ, Hu KL, Zhou JB, Tong LL and Tong LM (2010) Early carboniferous volcano magmatism and related mineralization in Yishijilike mountain, Western Tianshan. *Earth cience* **35**, 235–44 (in Chinese with English abstract).

Li YJ, Li ZC, Zhou JB, Gao ZH, Gao YL, Tong LM and Liu J (2009) Division of the carboniferous lithostratigraphic units in Awulale area, Western Tianshan. *Acta Petrologica Sinica* **25**, 1332–40 (in Chinese with English abstract).

Litvinovsky BA, Jahn BM, Zanvilevich AN, Saunders A and Poulain S (2002) Petrogenesis of syenite–granite suites from the Bryansky Complex (Transbaikalia, Russia): implications for the origin of A-type granitoid magmas. *Chemical Geology* **198**, 105–33.

Liu R and Chen GW (2018) Characteristics of rare earth elements, Zr, and Hf in ore-bearing porphyries from the Western Awulale Metallogenic Belt, Northwestern China and their application in determining metal fertility of granitic magma: REEs, Zr and Hf in ore-bearing porphyries. *Resource Geology* **69**, 193–210.

Liu R and Chen GW (2020) The 109 porphyry Cu deposit in the western Tianshan orogenic belt, NW China: an example of Cu mineralization in a reduced magmatichydrothermal system in an extensional setting. *Ore Geology Reviews* **111**, 102989.

Liu R, Chen GW and Yang JX (2020) Compositions of Cu-(Fe)-sulfides in the 109 reduced granite-related Cu deposit, Xinjiang, northwest China: implications on the characteristics of ore-forming fluids. *Geofluids*. doi: 10.1155/2020/7391369.

Liu R, Wang LX and Chen GW (2016) Genesis, geological significance and metallogentic potentiality of A-type granites in the Awulale area of the western Tianshan, Xinjiang. *Acta Petrologica Sinica* **33**, 1741–1754 (in Chinese with English abstract).

Long LL, Gao J, Klemd R, Beier C, Qian Q, Zhang X, Wang JB and Jian T (2011) Geochemical and geochronological studies of granitoid rocks from the WesternTianshan Orogen: implications for continental growth in the southwestern Central Asian orgenic belt. *Lithos* **126**, 321–40.

Long LL, Wang YW, Tang PZ, Wang LJ, Wang JB and Liao Z (2012) A debate on the special circumstance of rock-forming and ore-forming of Haladala pluton, a mafic-ultramafic complex related to Cu Ni-VTi Fe composite mineralization, in western Tianshan. *Acta Petrologica Sinica* **28**, 2015–28.

Mahoney JJ, Frei R, Tejada MLG, Mo XX, Leat PT and Nägler TF (1998) Tracing the Indian Ocean mantle domain through time: isotopic results from old West Indian, East Tethyan, and South Pacific seafloor. *Journal of Petrology* **39**, 1285–306.

Mahoney JJ, Saunders AD, Storey M and Randriamanantenasoa A (2008) Geochemistry of the Volcan de l'Androy basalt–rhyolite complex, Madagascar cretaceous igneous province. *Journal of Petrology* **49**, 1069–96.

Mao QG, Xiao WJ, Han CM, Yuan C and Sun M (2008) Late Paleozoic southward hyperplasia in the eastern Junggar region: implications from A-type granite. *Journal of Rocks* **24**, 733–42.

Martin H, Smithies RH, Rapp R, Moyen JF and Champion D (2005) An overview of adakite, tonalite-trondhjemite granodiorite (TTG), and sanukitoid: relationships and some implications for crustal evolution. *Lithos* **79**, 1–24.

Menzies MA, Fan W and Zhang M (1993) Palaeozoic and Cenozoic lithoprobes and the loss of >120 km of Archaean lithosphere, Sino-Korean craton, China. In *Magmatic Processes and Plate Tectonics* (ed. HM Prichard), pp. 71–81. Geological Society of London, Special Publication no. **76**.

Mitchell AL and Grove TL (2015) Melting the hydrous, subarc mantle: the origin of primitive andesites. *Contributions to Mineralogy and Petrology* **170**, 1–23.

Ning WT, Li YJ, Wang, ZY, Wang ZP and Li GY (2019) Geochemical characteristics of the bimodal volcanic rocks in Upper Carboniferous Yishijilike Formation in Tekes Daban area of Yining landmass. *Acta Petrologica et Mineralogica* **38**, 3–22 (in Chinese with English abstract).

Pearce JA (1991) Ocean floor comes ashore. *Nature* **354**, 110–11.

Pearce JA (2008) Geochemical fingerprinting of oceanic basalts with applications to ophiolite classification and the search for Archean oceanic crust. *Lithos* **100**, 14–48.

Pearce JA, Thirlwall MF, Ingram G, Murton BJ, Arculus RJ and Van der Laan S R (1992) Isotopic evidence for the origin of boninites and related rocks drilled in the Izu-Bonin (Ogasawara) forearc, Leg 125. *Proceedings of the Ocean Drilling Program, Scientific Results* **125**, 237–61.

Qian Q, Gao J, Klemd R, He GQ, Song B, Liu DY and Xu RH (2009) Early Paleozoic tectonic evolution of the Chinese South Tianshan Orogen: constraints from SHRIMP zircon U–Pb geochronology and geochemistry of basaltic and dioritic rocks from Xiate, NW China. *International Journal of Earth Sciences* **98**, 551–69.

Qian Q, Gao J, Xiong XM, Long LL and Huang DZ (2006) Petrogenesis and tectonic settings of Carboniferous volcanic rocks from north Zhaosu, western Tianshan Mountains: constraints from petrology and geochemistry. *Acta Petrologica Sinica* **22**, 1307–23 (in Chinese with English abstract).

Sajona FG, Maury RC, Bellon H, Cotten J, Defant M and Pubellier M (1993) Initiation of subduction and the generation of slab melts in the western and eastern Mindanao, Philippines. *Geology* **21**, 1007–1010.

Sheth HC and Melluso L (2008) The Mount Pavagadh volcanic suite, Deccan Traps: geo-chemical stratigraphy and magmatic evolution. *Journal of Asian Earth Science* **32**, 5–21.

Sun S and McDonough W (1989) Chemical and isotopic systematics of ocean basalts: implications for mantle composition and processes.. In *Magmatism in the Ocean Basins* (eds D Saunders and JM Norry), pp. 313–45. Geological Society of London, Special Publication no. 42.

Tang GJ, Chen HH, Wang Q, Zhao ZH, Wyman DA, Jiang ZQ and Jia XH (2008) Formation age and tectonic setting of the Dabat A-type granite in the Western Tianshan Mountains. *Acta Petrologica Sinica* **24**, 947–58 (in Chinese with English abstract).

Tong Y, Wang T, Hong D, Han BF, Zhang JJ, Shi XJ and Wang C (2010) Carboniferous-Permian granite in northern Xinjiang and adjacent areas: temporal and spatial distribution characteristics and their tectonic significance. *Journal of Rock Mineralogy* **29**, 619–41 (in Chinese with English abstract).

Turner S, Sandiford M and Foden J (1992) Some geodynamic and compositional constraints on 'postorogenic' magmatism. *Geology* **20**, 931–4.

Wang B, Faure M, Cluzel D, Shu L, Charvet J, Meffre S and Ma Q (2006) Late Paleozoic tectonic evolution of the northern West Chinese Tianshan belt. *Geodinamica Acta* **19**, 237–47.

Wang B, Liu HS, Shu LS, Jahn BM, Chung SL, Zhai YZ and Liu DY (2014) Early Neoproterozoic crustal evolution in northern Yili block: insights from migmatite, orthogneiss and leucogranite of the Wenquan metamorphic complex in the NW Chinese Tianshan. *Precambrian Research* **242**, 58–81.

Wang B, Shu LS, Cluzel D, Faure M and Charvet J (2007) Geochemical constraints on Carboniferous volcanic rocks of the Yili Block (Xinjiang, NW China): implication for the tectonic evolution of Western Tianshan. *Journal of Asian Earth Sciences* **29**, 148–59.

Watson EB and Harrison TM (1983) Zircon saturation revisited: temperature and composition effects in a variety of crustal magma types. *Earth and Planetary Science Letters* **64**, 295–304.

Whalen JB, Currie KL and Chappell BW (1987) A-type granites: geochemical characteristics, discrimination and petrogenesis. *Contributions to Mineralogy and Petrology* **95**, 407–19.

Wilson M (1989a) *Igneous Petrogenesis*. London: Unwin Hyman.

Wilson M (1989b) *Igneous Petrogenesis: A Global Tectonic Approach*. Dordrecht: Springer.

Windley BF, Allen MB, Zhan C, Zhao ZY and Wang GR (1990) Paleozoic accretion and Cenozoic redeformation of the Chinese Tien Shan range, central Asia. *Geology* **18**, 128–31.

Xia H, Chen GW, Liu Q and Luo Y (2011) Geochemical characteristics of the Dahalajunshan formation volcanic rocks in the Tulasu basin of Western Tianshan and its tectonic implication. *Geotectonica et Metallogenia* **130**, 429–38 (in Chinese with English abstract).

Xia LQ, Xu XY, Xia ZC, Li XM, Ma ZP and Wang LS (2004) Petrogenesis of Carboniferous rift-related volcanic rocks in the Tianshan, Northwestern China. *Geological Society of America Bulletin* **116**, 419–33.

Xiao WJ, Kröner A and Windley B (2009) Geodynamic evolution of Central Asia in the Paleozoic and Mesozoic. *International Journal of Earth Sciences* **98**, 1185–1188.

Xiao WJ, Windley BF, Allen M and Han CM (2013) Paleozoic multiple accretionary and collisional tectonics of the Chinese Tianshan orogenic collage. *Gondwana Research* **23**, 1316–41.

Xu XY, Ma ZP, Xia LQ, Wan YB, Li XM, Xia ZC and Wang LS (2005) SHRIMP dating of plagiogranite from Bayingou ophiolite in the Northern Tianshan Mountains. *Geological Review* **51**, 523–7 (in Chinese with English abstract).

Xu XY, Xi LQ, Ma ZP, Wan YB, Li XM, Xia ZC and Wang LS (2006) SHRIMP zircon U–Pb geochronology of the plagiogranites from Bayingou ophiolite in North Tianshan Mountains and the petrogeneis of the ophlolite. *Acta Petrologica Sinica* **22**, 83–94 (in Chinese with English abstract).

Yang GX, Li YJ, Kerr AC and Tong LL (2018) Accreted seamounts in North Tianshan, NW China: implications for the evolution of the Central Asian Orogenic Belt. *Journal of Asian Earth Sciences* **153**, 223–37.

Yang GX, Li YJ, Si GH, Wu HG, Jin C and Zhang YZ (2010) Zircon LA-ICPMS U-Pb dating and geological significance of the Belle Kuduk rock mass in the East Karamay area. *Geotectonica et Metallogenia* **34**, 133–8 (in Chinese with English abstract).

Yang JH, Sun JF, Chen F, Wilde SA and Wu FY (2007) Sources and petrogenesis of Late Triassic dolerite dikes in the Liaodong Peninsula: implications for post-collisional lithosphere thinning of the eastern North China Craton. *Journal of Petrology* **48**, 1973–97.

Yang JH, Wu FY, Chung SL, Wilde SA and Chu MF (2006) A hybrid origin for the Qianshan A-type granite, northeast China: geochemical and Sr–Nd–Hf isotopic evidence. *Lithos* **89**, 89–106.

Yao JY (1993) Geological characteristics of continental volcanic-hosted copper deposits in the Western section of the Mt. Awulale, Xinjiang. *Geological Exploration for Non-Ferrrous Metals* **2**, 277–83 (in Chinese with English abstract).

Zhang LQ, Zhang HF, Zhang SS, Xiong ZL, Luo BJ, Yang H, Pan FB, Zhou XC, Xu WC and Guo L (2017) Lithospheric delamination in post-collisional setting: evidence from intrusive magmatism from the North Qilian orogeny to southern margin of the Alxa block, NW China. *Lithos* **288–289**, 20–34.

Zhang XH, Zhang H, Tang Y, Wilde SA and Hu Z (2008) Geochemistry of Permian bimodal volcanic rocks from central Inner Mongolia, North China: implication for tectonic setting and Phanerozoic continental growth in Central Asian Orogenic Belt. *Chemical Geology* **249**, 262–81.

Zhang ZH, Wang ZL, Wang LS and Zuo GC (2010) Metallogenic epoch and ore-forming environment of the Lamasu skarn-porphyritic Cu-Zn deposit, western Tianshan, Xinjiang, NW China. *Acta Geologica Sinica* **82**, 731–40.

Zhao J, Zhang ZH, Zhang H, Liu M, Hong W and Jiang ZS (2013) Geochemistry petrogenesis and tectonic setting of the Lower Permian series volcanic rocks from western Awulale Mountain, Xinjiang. *Acta Geologica Sinica* **87**, 525–41 (in Chinese with English abstract).

Zhao ZH, Wang Q, Xiong XL, Zhang HY, Niu HC, Xu JF, Bai ZH and Qiao YL (2006) Two types of adakites in north Xinjiang, China. *Acta Petrologica Sinica* **22**, 1249–1260 (in Chinese with English abstract).

Zhao ZH, Xiong XL, Wang Q, Bai ZH and Qiao YL (2009) Late Paleozoic underplating in North Xinjiang: evidence from shoshonites and adakites. *Gondwana Research* **16**, 216–26.

Zhu YF, Zhang L, Gu L, Guo X and Zhou J (2005) The zircon SHRIMP chronology and trace element geochemistry of the Carboniferous volcanic rocks in western Tianshan Mountains. *Chinese Science Bulletin* **50**, 2201–12.

Zhu ZX, Li J, Dong LH, Wang KZ, Zhang XF and Xu SQ (2011) Geological characteristics and tectonic significance of Paleozoic intrusive rocks in Western Tianshan of Xinjiang Uygur Autonomous Region. *Earth Science Frontier* **18**, 170–9 (in Chinese with English abstract).

https://doi.org/10.1017/S0016756820001090 Published online by Cambridge University Press